AD-A124 640 NEW MEASUREMENT TECHNIQUES USING TRACERS WITHIN LASER-PRODUCED PLASMAS(U) NAVAL RESEARCH LAB WASHINGTON DC M J HERBST ET AL. 06 JAN 83 NRL-MR-5003 1/1

UNCLASSIFIED F/G 20/9 NL

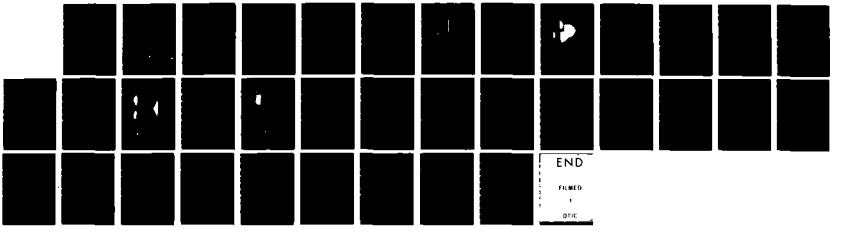

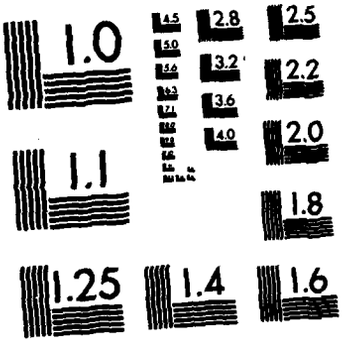

NRL Memorandum Report 5003

New Measurement Techniques Using Tracers Within Laser-Produced Plasmas

M. J. HERBST, P. G. BURKHALTER,* D. DUSTON,† M. EMERY,§
J. GARDNER,§ J. GRUN,‡ S. P. OBENSCHAIN, B. H. RIPIN,
R. R. WHITLOCK,* J. P. APRUZESE,† AND J. DAVIS†

Laser Plasma Branch
Plasma Physics Division

**Condensed Matter Physics Branch*
Condensed Matter and Radiation Sciences Division

†*Plasma Radiation Branch*
Plasma Physics Division

‡*Mission Research Corporation*
Alexandria, VA

§*Laboratory for Computational Physics*

January 6, 1983

This work is supported by the U.S. Department of Energy, Office of Naval Research, and Defense Nuclear Agency under Subtask I25BMXIO, work unit 00015, and work unit title "Laser Plasma HANE Simulation Experiment."

This paper was prepared for presentation at the Sixth International Workshop on Laser Interaction and Related Plasma Phenomena held in Monterey, CA on October 25—29, 1982.

NAVAL RESEARCH LABORATORY
Washington, D.C.

SECURITY CLASSIFICATION OF THIS PAGE (When Data Entered)

REPORT DOCUMENTATION PAGE	READ INSTRUCTIONS BEFORE COMPLETING FORM
1. REPORT NUMBER: NRL Memorandum Report 5003	2. GOVT ACCESSION NO.: AD-A124640
	3. RECIPIENT'S CATALOG NUMBER:
4. TITLE (and Subtitle): NEW MEASUREMENT TECHNIQUES USING TRACERS WITHIN LASER-PRODUCED PLASMAS	5. TYPE OF REPORT & PERIOD COVERED: Interim report on a continuing NRL problem.
	6. PERFORMING ORG. REPORT NUMBER:
7. AUTHOR(s): M.J. Herbst, P.G. Burkhalter, D. Duston, M. Emery, J. Gardner, J. Grun*, S.P. Obenschain, B.H. Ripin, R.R. Whitlock, J.P. Apruzese and J. Davis	8. CONTRACT OR GRANT NUMBER(s):
9. PERFORMING ORGANIZATION NAME AND ADDRESS: Naval Research Laboratory, Washington, DC 20375	10. PROGRAM ELEMENT, PROJECT, TASK AREA & WORK UNIT NUMBERS: DOE AI08-79DP 40092(172); 47-0859-0-3; DNA 62715H; 47-1606-0-3
11. CONTROLLING OFFICE NAME AND ADDRESS: U. S. Department of Energy, Washington, DC 20545	12. REPORT DATE: January 6, 1983
	13. NUMBER OF PAGES: 35
14. MONITORING AGENCY NAME & ADDRESS(if different from Controlling Office)	15. SECURITY CLASS. (of this report): UNCLASSIFIED
	15a. DECLASSIFICATION/DOWNGRADING SCHEDULE:

16. DISTRIBUTION STATEMENT (of this Report)

Approved for public release; distribution unlimited.

17. DISTRIBUTION STATEMENT (of the abstract entered in Block 20, if different from Report)

18. SUPPLEMENTARY NOTES

*Present address: Mission Research Corporation, Alexandria, VA

This work is supported by the U.S. Department of Energy, Office of Naval Research and Defense Nuclear Agency under Subtask I25BMXEO, work unit 00015, and work unit title "Laser Plasma HANE Simulation Experiment."

(Continues)

19. KEY WORDS (Continue on reverse side if necessary and identify by block number)

Plasma diagnostics
Laser-plasma interactions
X-ray spectroscopy
Fluid flow visualization
Rayleigh-Taylor instability

20. ABSTRACT (Continue on reverse side if necessary and identify by block number)

The use of locally embedded tracers within laser-irradiated solid targets has led to a new class of diagnostic methods for laser-produced plasmas. Demonstrated uses of tracers include the first visualizations of hydrodynamic flow of laser-ablated material and improved spectroscopic measurements of plasma density and temperature profiles; comparisons with a two-dimensional hydrodynamics computer code are shown. Proposed future uses of tracers include the first measurements of fluid velocity profiles and improved determinations of mass ablation rates.

DD FORM 1 JAN 73 1473 EDITION OF 1 NOV 65 IS OBSOLETE
S/N 0102-014-6601

SECURITY CLASSIFICATION OF THIS PAGE (When Data Entered)

18. Supplementary Notes (Continued)

This paper was prepared for presentation at the Sixth International Workshop on Laser Interaction and Related Plasma Phenomena held in Monterey, CA on October 25—29, 1982.

CONTENTS

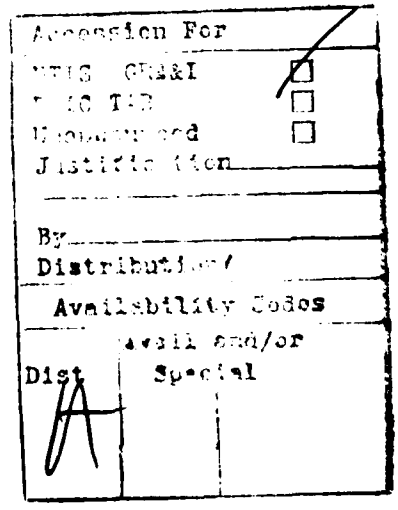

NEW MEASUREMENT TECHNIQUES USING TRACERS WITHIN LASER-PRODUCED PLASMAS

I. INTRODUCTION

Many of the physical processes which are important to the ablative-compression approach to laser-pellet fusion are intimately related to plasma density, temperature, and velocity profiles. Inverse bremsstrahlung absorption and parametric instabilities are closely coupled with underdense plasma profiles. Similarly, energy transport between the critical density surface and the ablation surface is interrelated with overdense plasma profiles. Therefore, laser-plasma interaction experiments can better address these physics issues if they include measurements of the plasma profiles. If experiments are performed in planar rather than spherical geometry, the problem becomes two-dimensional since the plasma profiles and the above-mentioned physical processes are affected by lateral flow of energy out of the finite focal spot. One then desires measurements of the area over which the absorbed energy is distributed and, if possible, of both axial and lateral profiles.

A new genre of diagnostic methods is being developed at the Naval Research Laboratory to address these and other problems. The unique feature of these new methods is the use of tracer materials which are locally embedded into the solid target to be irradiated. Tracers which are localized within the focal region remain localized within the blowoff plasma, due to the collisional or fluid nature of the flow of material ablated from the target. By imaging characteristic radiation from a linear array of such tracer dots, we have demonstrated the first visualizations of the hydrodynamic flow of material within laser produced plasmas;[1] this technique and its applications are discussed in Sec. II. As described in Sec. III, improved measurements of plasma density and temperature profiles have also been demonstrated, by using the tracer dots as local sources of spectroscopic diagnostic lines.[2] Comparisons with these measurements provide the most direct calibration of hydrodynamics computer codes, because plasma profiles are the experimental observables most closely coupled to mechanisms of energy absorption and transport in laser-produced plasmas. Therefore, comparisons between experiments and the Naval Research Laboratory hydro-codes are found throughout Secs. II and III. In Sec. IV, the use of layered tracer spots is proposed for time-resolved measurements of fluid velocity profiles[3] and for improved measurements of mass ablation rates.

II. FLUID FLOW VISUALIZATIONS AND THEIR USES

The simplest use of tracer dots is for visualization of the hydrodynamic flow of material from the laser irradiated target, for which the experimental arrangement is as shown in Fig. 1. The distinguishing feature of this configuration is the target: thick polystyrene $[(CH)_x]$ with a linear array of 25 μm diameter, aluminum tracer dots. These dots are embedded so that their initial surfaces are flush with that of the surrounding target, and their thicknesses are chosen to exceed the expected ablation depth on any given shot. With the tracer spots aligned to fall along a diameter of the laser-irradiated region, between 10 and 500 J of Nd-laser energy (λ = 1.054 μm) is brought onto the target in a 3-5 nsec pulse. A camera with an array of pinholes is used to obtain time-

Manuscript approved December 9, 1982.

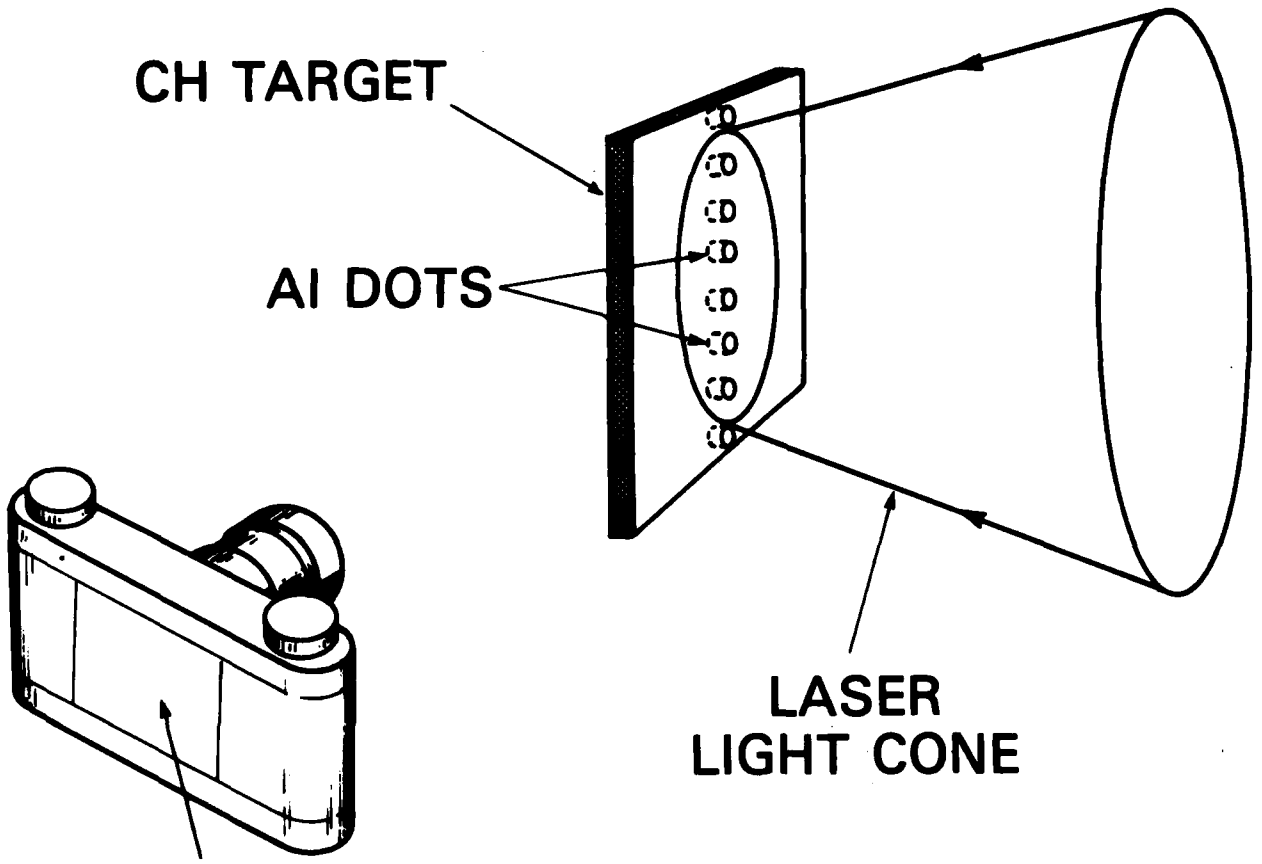

Fig. 1 Experimental configuration for visualization of hydrodynamic flow.

integrated images of x-ray emission at 90° to the target normal. The 15 μm beryllium filter used on the camera allows imaging of photons with energy $h\nu > 1$ keV. Since aluminum line emission is more intense than carbon or hydrogen continuum emission in the spectral band of the pinhole camera, streamlines of material flowing from the aluminum spots are identifiable as tracks of strong x-ray emission in the images (see Fig. 2).

Flow visualization experiments have been performed at a variety of laser focal conditions with incident intensities I_{90} (averaged within the 90% energy-content diameter d_{90}) between 10^{12} and 2×10^{14} W/cm^2. On each shot, a series of laser isointensity patterns is recorded in an equivalent focal plane to that of the target,[4] with a factor of 2.2 in intensity between successive patterns. From these records, we may plot focal intensity distributions, such as those shown in Fig. 3. (These one-dimensional profiles represent azimuthal averages of the real two-dimensional profiles of the laser; these are used as input to the hydrocodes.) Note that the focal distribution near best focus of our f/6 lens is qualitatively different from that in the quasi-near field. The most obvious difference is near the center of the distribution, where large focal spots tend to exhibit local minima in intensity. Equally important, however, are differences in the wings of the distributions, as will be discussed in Sec. II.B. It should also be noted that intensities I_{50} (averaged over 50% energy content diameter d_{50}) and I_{pk} (peak intensity) tend to be higher than I_{90} by factors of 2 and 4, respectively.

While we have not conclusively demonstrated that the presence of the tracers does not perturb the visualized flow, there is some evidence that the perturbation should be minimal. First, the fully ionized mass densities for Al and $(CH)_x$ differ by only 12% at a given electron density in the blowoff plasma. Moreover, the average velocity of ablated ions as determined by Faraday cups is the same for the two materials.

In the following sections, the various physics issues that may be addressed by flow visualization methods are discussed. The shape of the visualized flows, as shown in Sec. II.A, is related to the outward hydrodynamic flow of plasma, and provides a valuable check for the hydrodynamics codes. In Sec. II.B, we present the observed sizes of the fluid sources under various irradiation conditions; this should indicate the degree to which absorbed laser energy spreads laterally as it flows inward from the absorption region to the ablation region near the edges of the focal spot. Lateral energy transport can also be important near the center of the focal spot if the irradiation there is nonuniform.[5,6] Flow visualizations obtained with intentionally perturbed laser beams qualitatively show this effect,[6] as described in Sec. II.C. Another proposed application for these flow visualizations, outlined in the final section, is for diagnosis of the Rayleigh-Taylor instability.[7]

A. Shape of the Visualized Flows

While the size of the observed fluid source varies with laser intensity and spot size, the shape of the flow pattern seems to be remarkably constant. As shown in Fig. 2, streamlines curve away from the

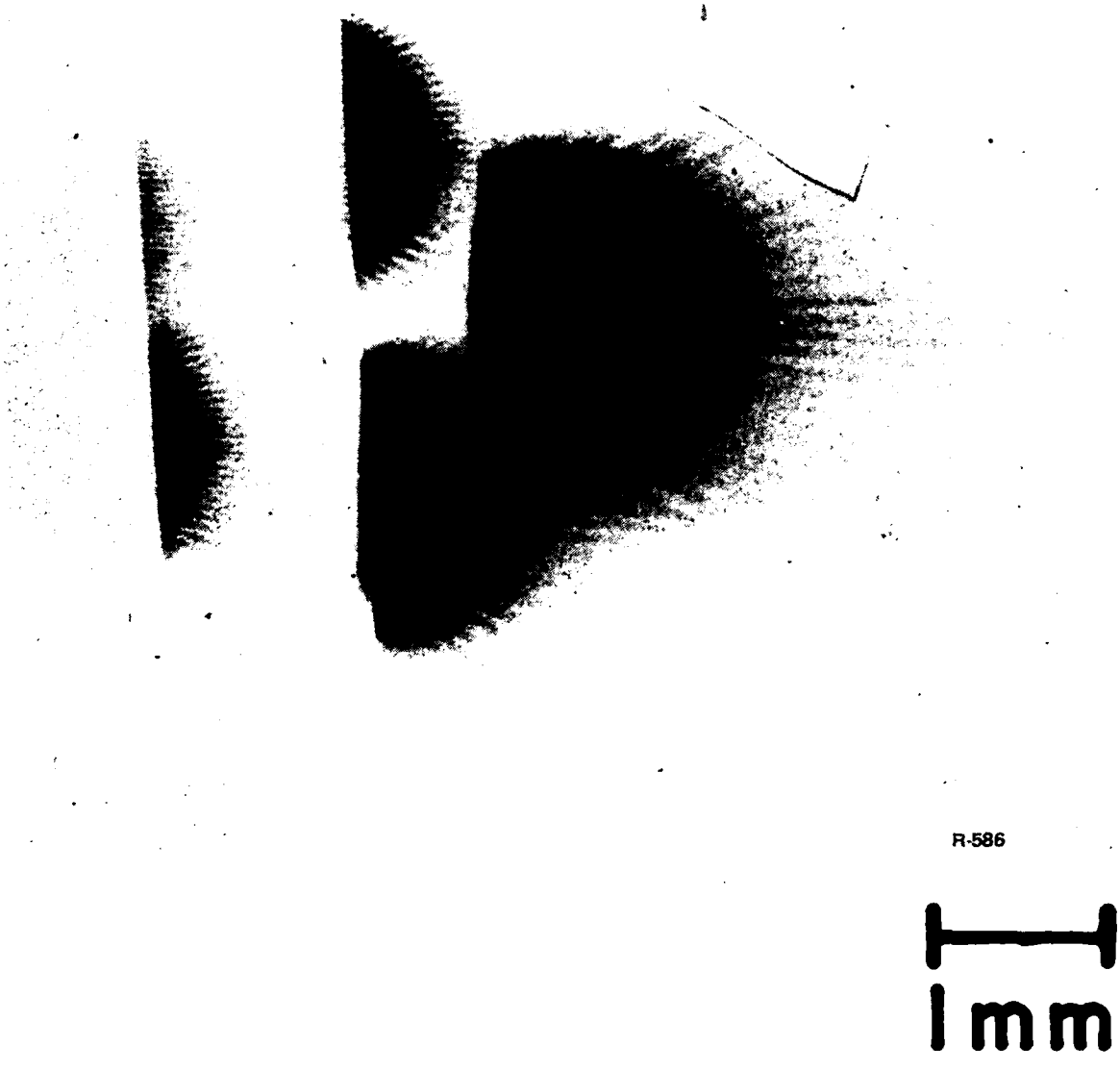

Fig. 2 Five flow visualizations obtained on a single shot with 5, 9, 13, 28, and 54 μm diameter pinholes. The laser is incident from the right, and the target surface is to the left. $I_{90} \approx 3.2 \times 10^{12}$, $d_{90} \approx 1470$ μm, and the laser energy is 212 J.

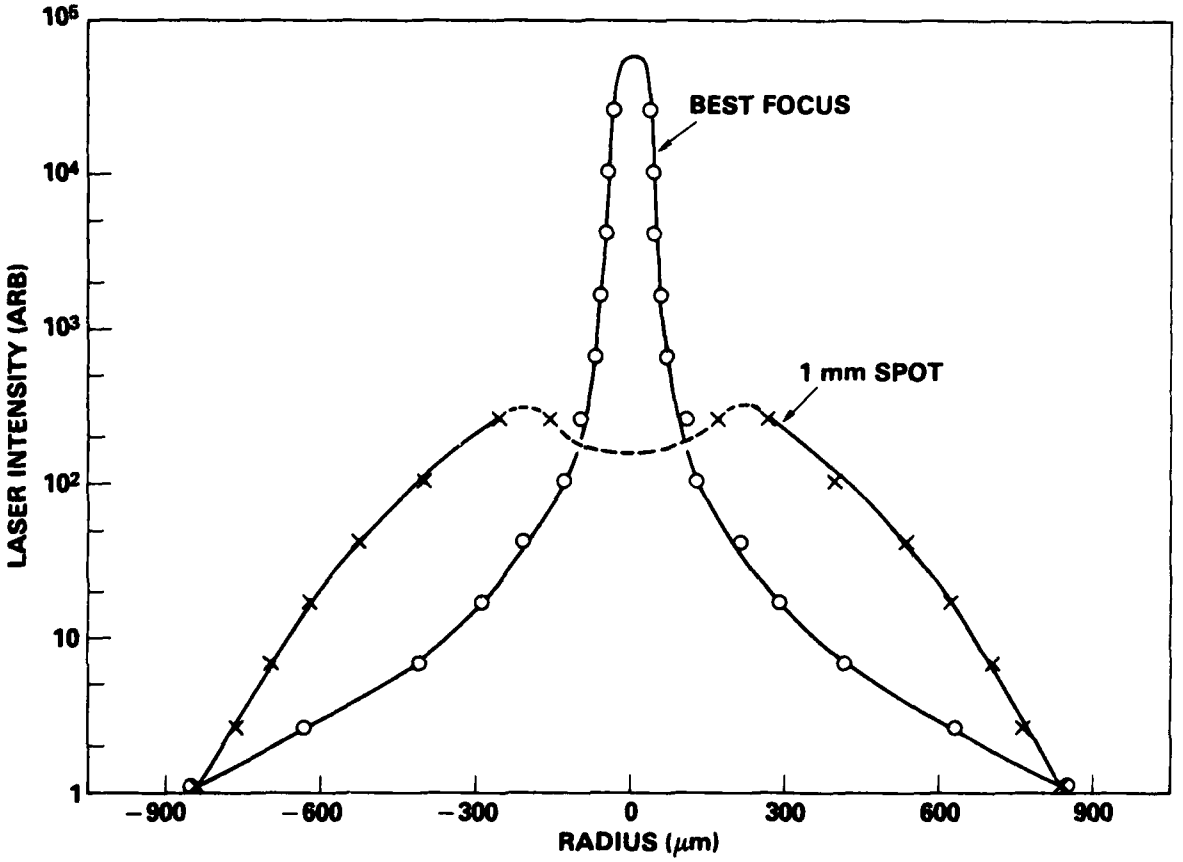

Fig. 3 Azimuthally averaged laser energy profiles for best focus of our f/6 lens and position in the quasi-near field where $d_{90} \approx 1075$ μm.

target normal at a rate which depends upon r/r_0, where r is the displacement of a given streamline from the center of the fluid source and r_0 is the radius of the fluid source. Each streamline attains a constant direction within a distance $z \approx r$ from the target surface; beyond $z \approx r_0$, all streamlines are following straight-line paths corresponding to a far-field, spherically diverging flow.

The shape of the visualized flows is in good agreement with NRL's two-dimensional hydrodynamics codes. As shown in Fig. 4, the measured streamline angles θ relative to the target normal are well predicted by a cylindrical (r and z) hydrodynamics simulation of the experiment. The computer model, described elsewhere in these proceedings,[8] uses a sliding-grid Eulerian mesh with flux-corrected transport, classical $T^{5/2}$ thermal conduction, and inverse bremsstrahlung absorption. The calculation uses the measured laser pulse duration and an azimuthal average of the measured laser focal distribution (such as those in Fig. 3). The slight asymmetry of the experimental data about r = 0 is a gentle reminder that real laser profiles are not perfectly symmetric, but prohibitively expensive, three-dimensional codes would be required to accurately simulate such focal nonuniformities. While Fig. 4 shows agreement at one distance z from the target, sets of such plots at varying z convince us that the code is correctly calculating the shape of the flow.

The fluid nature of the flow is not surprising, since the plasma radii are much greater than the ion-ion collision mean free path. The fact that time-integrated flow visualizations compare well with snapshots of the code, as in Fig. 4, suggests that we may also have a nearly steady flow; this is not entirely unreasonable, since the laser pulse length exceeds the acoustic transit time across a plasma radius. Experimental evidence that the flow is nearly steady, at least during the period of maximal x-ray emission, is obtained from streak photography of images of $3/2\omega_0$ emission from the $n_c/4$ surface.[9] The position along the laser axis of this surface appears relatively stationary for the duration of the $3/2\omega_0$ emission, a period of up to 3 nsec near the time of peak laser intensity.

The shape of the flow affects far-field particle diagnostics such as ion collectors or plasma calorimeters. First, the angular distribution of ablated mass observed by these diagnostics may be determined by the collisional flow near the target, which imparts a fluid velocity direction to each fluid element. As the material drifts through the collisionless region further from the target, some lateral spreading of material results from random thermal motions; since directed ablation velocities are generally much greater than ion thermal velocities, this should not greatly increase the angular range set by the fluid flow. Indeed, charge collector and plasma calorimeter measurements indicate that half of the ablated mass appears in a cone about the target normal with a 40° half-angle;[10] this is consistent with the angular spread inferred from flow visualizations.

Ion detectors are further affected because the flow, except for any smearing due to thermal expansion in the collisionless region, maps different regions of target surface into different diagnostic solid angles. A single ion detector at a specific angle far from the target then

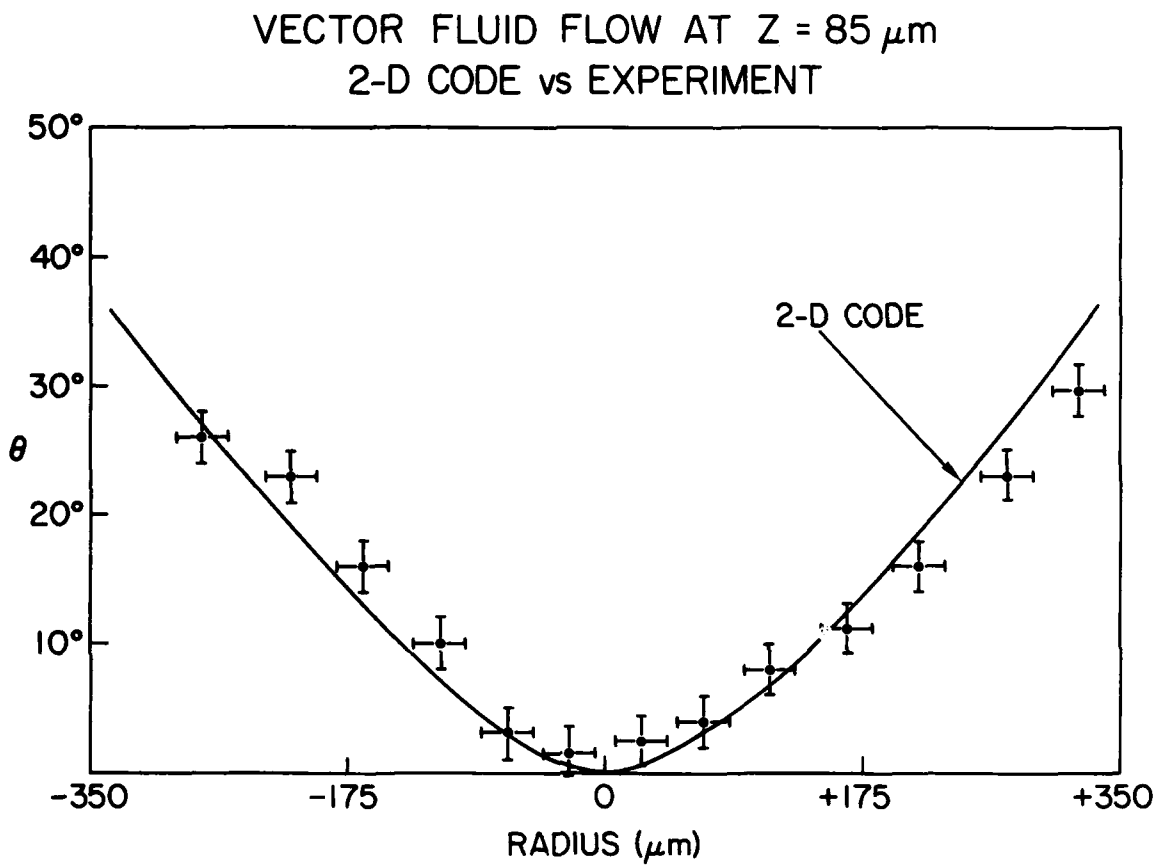

Fig. 4 Comparison between measured and calculated streamline angles θ relative to the target normal as functions of the radial displacement from the center of the flow. Values are taken at one distance z = 85 μm from the target surface. The calculation uses measured experimental conditions: $I_{90} \approx 2 \times 10^{12}$ W/cm^2, $d_{90} \approx 650$ μm, laser energy is 35 J.

samples only a portion of the irradiated region. To measure parameters averaged over the focal spot, one should use an array of detectors at a range of angles. The error that may result if too few detectors are used depends upon the uniformity of the laser illumination at the target, the ratio of the directed ablation velocity to the ion thermal velocities, and the solid angle subtended by the detectors used.

B. Sizes of the Visualized Flows

The sizes of the visualized flows are well-defined and useful observables. From the flow visualizations, we define the fluid source size to be the diameter of the region at the target surface from which streamlines are seen to emanate. This quantity does have physical significance; as discussed below, it most likely reflects the diameter within which the plasma temperature is high enough for excitation of Al K-lines. It is also a well-defined quantity, in the sense that it is not extremely sensitive to the size of pinhole used to detect the x-rays. As seen in Fig. 2, the same number of streamlines is observed in the three largest pinhole images, despite a factor of 17 variation in pinhole collection efficiency. This may indicate the rapidity with which the temperature is falling at the edge of the x-ray images. The advantage of this observable over the size of standard pinhole images lies mainly in the ease of observation. The size of standard images is usually sensitive to pinhole size. In order to define a plasma size, one must densitometer the images, deconvolve the pinhole size, and invert the data to obtain isointensity contours of x-ray emission.

The observed fluid source diameter d_0 varies with laser intensity and spot size. As indicated in Fig. 5, d_0 increases with laser energy at fixed spot size and increases with spot size at fixed laser energy. One interesting observation is that the sensitivity of d_0 to laser energy is greater for the smaller focal spot sizes. Several possible explanations exist for such an observation: there is the potential effect of higher lateral thermal conductivity, which could result from higher plasma temperatures at the higher intensities, as well as the possibility of increased lateral flow due to fast electrons. A closer look at the shapes of the wings of the laser focal distributions in Fig. 3 suggests another explanation. By locating the position within the focal distributions at which a given intensity occurs and plotting the variation of that position with increasing laser energy, we generate curves such as shown in Fig. 5. Within experimental uncertainty (approximately a factor of 2), the intensity for both curves shown in Fig. 5 is 2×10^{11} W/cm^2. The correlation with the data points suggests that the edge of the fluid source consistently occurs at that particular intensity in the wings of the laser focal distribution. This could be explained by the existence of a threshold intensity for heating to a temperature at which the Al K-lines are excited; this heating could be directly due to laser energy deposition or could be due to laser heating to a temperature at which the thermal conductivity allows lateral transport of energy from higher intensity regions. It is not likely that intensity thresholds for ionization of the target play any role in determining the fluid source size, since the two-dimensional hydrodynamics codes calculate the flow pattern correctly (see

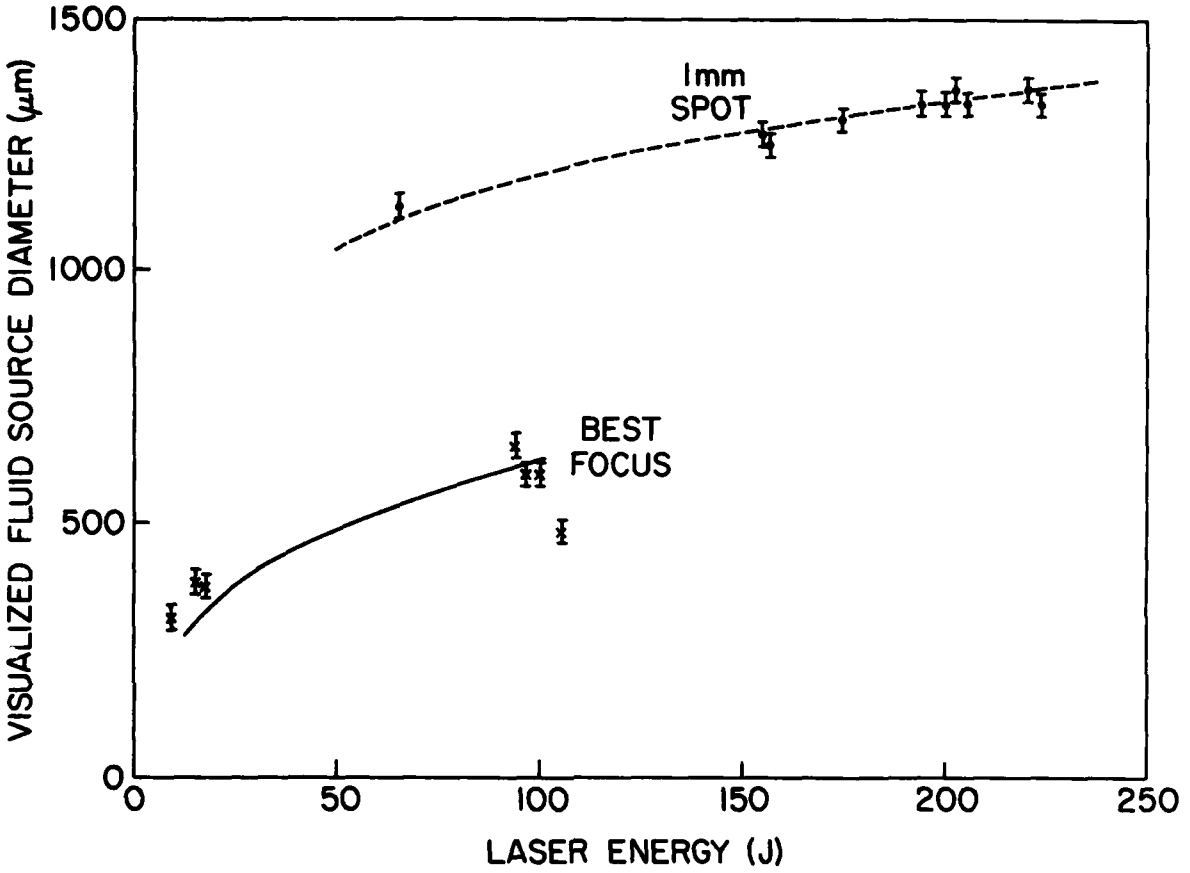

Fig. 5 Variation of fluid source diameter (data points) with laser energy for the two laser focal conditions shown in Fig. 3. Curves show the location of 2×10^{11} W/cm^2 intensity in the wings of the focal profile as function of laser energy for these same two focal conditions.

Fig. 4) while assuming initial ionization everywhere on the target.

If the fluid source size is entirely determined by the shape of the wings of the laser focal distribution, one might infer that the effects of lateral energy transport at the edges of the focal spot are minimal or that the lateral energy flow does not result in a high plasma temperature at the focal periphery. This empirical observation may be purely coincidental, however. Further comparisons should be made between the experiment and code at a variety of intensities and focal spot sizes before such a conclusion can be drawn.

C. Flow Visualizations with Intentionally Perturbed Laser Intensity Distributions

Lateral energy transport between absorption and ablation surfaces can also be addressed by flow visualizations in the presence of intentionally imposed laser nonuniformities. This diagnostic complements target acceleration experiments, where velocity modulations $\Delta v/v$ have been measured as a function of imposed intensity modulations $\Delta I/I$;[5,6,11] with the tracer technique one hopes to access the modulation in ablation pressure $\Delta P/P$ which couples $\Delta v/v$ to $\Delta I/I$.[6]

The idea is qualitatively illustrated in Fig. 6, where two flow visualizations are compared. The upper image is obtained with a deeper and wider intensity minimum imposed into the center of the focal distribution. Under these conditions, target acceleration results[5] indicate little smoothing of the intensity modulation by lateral thermal transport between absorption and ablation surfaces. Indeed, the flow visualization shows two seemingly independent fluid sources, with no detectable ablation from the central region where the intensity is low. In contrast, the lower image is obtained at higher average irradiance, with a shallower and narrower intensity minimum in the center of the beam; under these conditions, smoothing of the intensity modulation is observed in the target acceleration studies.[5] Flow is now seen from the center of the focal region, although compression of this region due to inward flow of surrounding streamlines indicates that there is residual pressure modulation. More quantitative analysis of pressure modulations requires comparisons of flow visualizations with the code or development of new techniques discussed in Sec. III.C.

D. Detection of the Rayleigh-Taylor Instability

Another potential use of the flow visualization method is for observation of hydrodynamic instability of accelerating targets.[7] Two-dimensional hydrodynamic simulations of foils unstable to Rayleigh-Taylor growth have shown that nonuniform ablation from the target surface accompanies the nonlinear state of the instability.[12] In the extreme limit of bubble-and-spike formation, these computer calculations show that all of the plasma flowing from the target can be emanating from the tips of the spikes, while none flows from the target surface in the regions of the bubbles. Preliminary flow visualization experiments have been performed to look for this nonuniform ablation,[7] using targets with periodically

Fig. 6 Sketch at left indicates the method used to impose a minimum in the center of the quasi-near field focal profile; a strip mask blocks the center of the lens. Upper flow visualization is obtained with $I_{90} \approx 3 \times 10^{12}$ W/cm^2 within $d_{90} \approx 1450$ μm and an approximate 8-to-1 intensity modulation in the center of the beam. Conditions for lower visualization are $I_{90} \approx 6 \times 10^{12}$ W/cm^2 within $d_{90} \approx 950$ μm and a 6 to 1 dip in the beam center.

perturbed areal densities to seed instability growth at given wavelengths.[13] The use of these perturbed targets also allows one to selectively deposit the tracers at locations which are expected to develop into the spikes of the unstable target; one can then look for the tracer material to appear everywhere in the blowoff, signifying the expected nonuniformity in ablation. These preliminary experiments have produced flow patterns which show qualitative deviations from the usual patterns, but they are not yet fully explained.[7]

III. SPOT SPECTROSCOPY: IMPROVED DENSITY AND TEMPERATURE MEASUREMENTS

A natural extension of the tracer technique is into the area of spectroscopic plasma diagnosis.[2] As pointed out in Sec. II, it is the strong line emission from the ablated tracer material which allows visualization of 25 μm diameter streamlines within 1 mm diameter plasmas. These emitted lines can also serve for spectroscopic measurements of plasma density and temperature.[14] The new technique, spot spectroscopy, has three major advantages over standard spectroscopic methods. Standard spectroscopic measurements are integrated along a diagnostic line of sight through an inhomogeneous plasma. One could use straightforward inversion techniques to obtain spatially resolved emissivities from the chord-integrated data if the plasmas were optically thin,[14] but effects of plasma opacity on the radiation exiting the plasma are non-negligible at the higher densities of interest.[15,16] A more complicated inversion technique might also account for the spatially varying opacity; however, the more typical procedure has been to predict the plasma profile with a hydrodynamics computer code and to compare the experimentally observed spectrum with those calculated for chord integrations across the inhomogeneous plasma.[17,18] In that case, one is dependent upon the correctness of the hydrodynamics model as well as the atomic physics model, and one would obviously prefer to make more direct determinations of density and temperature. Two of the three advantages of spot spectroscopy alleviate these problems of standard spectroscopy: 1) the localized source of spectroscopic lines should eliminate chord integration across an inhomogeneous plasma, and 2) the smaller source size also reduces complicating effects due to plasma opacity. The third advantage of spot spectroscopy is that better spectral resolution can be realized, since spectral resolution with standard x-ray spectroscopy is usually limited by source broadening due to finite plasma size.

A. The Experiment

Except for the presence of the tracer in the target, the experimental arrangement for the new technique is much the same as for standard x-ray spectroscopy. As shown in the illustration of Fig. 7, the target has a single aluminum tracer spot embedded in the center of the focal region; the variety of laser irradiation conditions used are the same as those used for the flow visualization technique (see Sec. II). Aluminum line radiation in the 5-8 Å spectral region is collected by an x-ray crystal spectrograph with a viewing axis parallel to the target surface. The spectrograph slit is oriented to yield spatial resolution in the direction along the laser

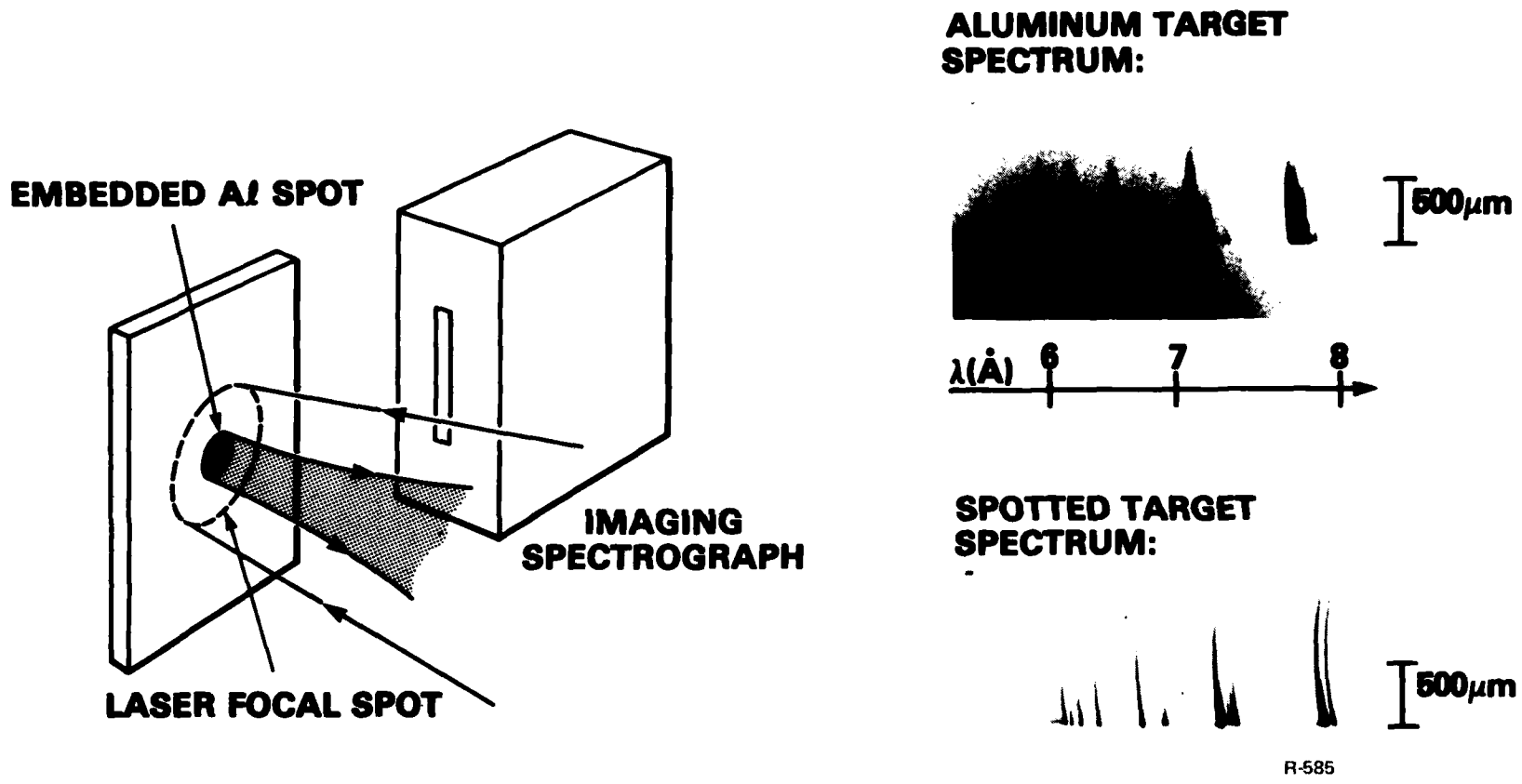

Fig. 7 Sketch at left shows experimental configuration for spot spectroscopy. The upper spectrum is obtained from an Al foil target with $I_{90} \simeq 8 \times 10^{12}$ W/cm^2 within $d_{90} \simeq 600$ μm and with a laser energy of 110 J. A $(CH)_x$ foil target with a 180 μm diameter, embedded Al spot is used to acquire the lower spectrum, with $I_{90} \simeq 8 \times 10^{12}$ W/cm^2 within $d_{90} \simeq 900$ μm and a laser energy of 225 J. The vertical axis for both spectra corresponds to the laser axis, with the laser incident from above and the target surface at bottom.

axis; resolution in the other two spatial dimensions results from the knowledge of the position of the localized tracer within the focal spot. The spectra are recorded on Kodak No-Screen film, for which a film model[19] based upon an absolute calibration[20] is available. A beryllium filter of nominally 15 μm thickness protects the film from visible exposure.

More specific conditions depend upon the goals of the particular experiment. As with standard x-ray spectroscopy, one may vary the crystal type and geometry, the spectrograph slit width and magnification, and the slit-to-target distance in order to achieve the optimal tradeoff between spectral resolution, spatial resolution along the laser axis, and sensitivity. An additional variable available with spot spectroscopy is the diameter of the embedded tracer; this allows one to specify spatial resolution in the direction lateral to the laser axis, but it also impacts achievable spectral resolution and sensitivity. The specific choice of parameters for the present work are the same as those listed in Ref. 2.

Data obtained with the new technique do show the expected improvement in spectral resolution. With an aluminum foil target, as shown in Fig. 7, the spectral widths of the lines near the target surface are quite broad; the widths exceed those expected for other broadening mechanisms, and reflect source broadening due to the large Al plasma extent transverse to the laser axis. Also shown in Fig. 7 is a spectrum obtained using a $(CH)_x$ target with an embedded Al dot. Line widths near the target surface are much narrower, and sets of lines are clearly resolved that are not resolved in the Al foil spectrum.

B. Density and Temperature Profiles

Several features of the experimental spectra may be used in determinations of plasma density and temperature. In the present work, we extract temperatures from intensity ratios of various helium-like (Al XII) ionic lines to hydrogen-like (Al XIII) ionic lines. These ratios are compared with calculated ratios from a cylindrical plasma/atomic physics model of a finite, homogeneous plasma with diameter equal to the measured tracer plasma diameter.[21] At least four methods exist for density determination: 1) the often-used technique based upon the ratio between the helium-like resonance and intercombination lines,[22] 2) a method based upon the ratio between two helium-like satellite lines ($1s2s\ ^3S \rightarrow 2s2p\ ^3P$ and $1s2p\ ^3P \rightarrow 2p^2\ ^3P$),[15] 3) Stark profile analysis of higher Rydberg members, and 4) profile analysis of opacity-broadened lines near the target surface. To date, we have exploited the first two methods, though we have discovered a need to modify the first method when comparing with the experiment; preliminary work is underway on the two remaining techniques.

A problem with previous models for density measurement is identified during data reduction.[23] Variations of intensity of various spectral features with distance from the target are plotted in Fig. 8. Plots are shown of the three strongest helium-like and hydrogen-like lines used in determining temperature, but the more important curve in the figure shows the variation of the ratio of the helium-like intercombination (He^3P) and resonance (He α) lines. As mentioned above, this ratio is routinely used

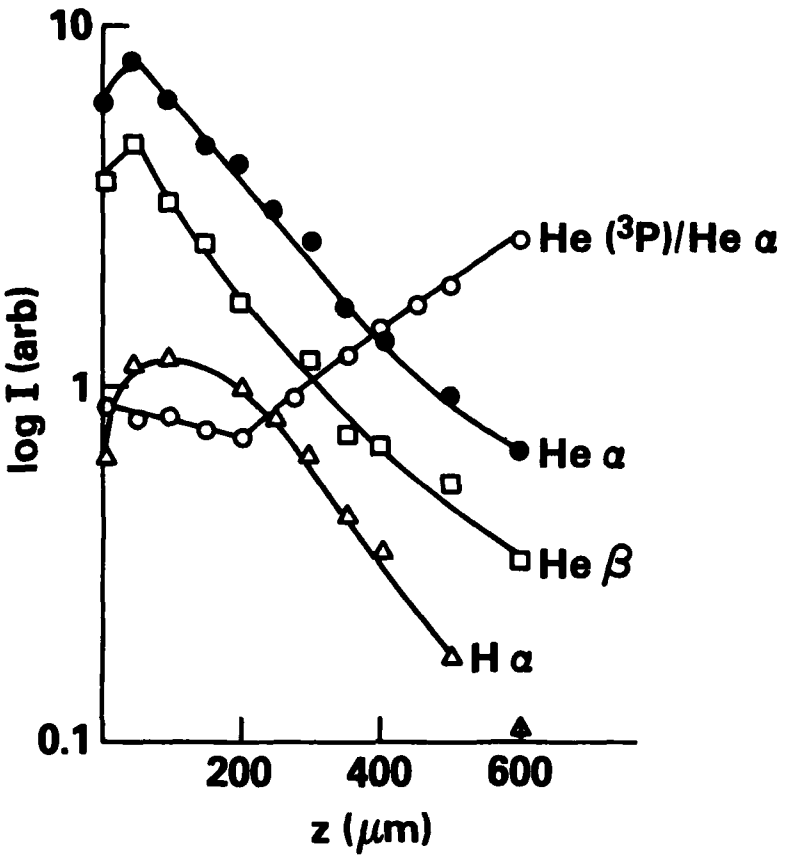

$I_{90} \approx 7.3 \times 10^{12} W/cm^2$ $d_{90} \approx 1$ mm $E = 273J$ $\tau_L = 4ns$ (11505)

Fig. 8 Variation of spectral intensities of helium-like α and β and hydrogen-like α Rydberg lines with distance z from target. Also shown is the variation of the ratio of the helium-like intercombination line to the resonance line. The target is $(CH)_x$ with a 65 μm diameter, embedded Al spot. $I_{90} \approx 7.3 \times 10^{12}$ W/cm^2 within $d_{90} \approx 1$ mm and the laser energy is 273 J.

for density measurement. Collisional-radiative equilibrium (CRE) models indicate that this ratio should fall monotonically with increasing density except for plasma opacity effects very near to the target.[21] For $z > 200$ μm, this expected behavior is observed and leads directly to measured densities up to 0.5 n_c. For $z < 200$ μm, however, we observe an apparent levelling off or even an increase in the line ratio; were we to naively apply previous models to this data, we would infer a density shelf of $n = 0.5\ n_c$ for $z \leq 200$ μm. With our improved spectral resolution, we can almost resolve satellite lines which nearly underlie the long-wavelength side of the intercombination line, and interfere with the intercombination intensity measurement. These lines, identified as the lithium-like s,t satellites [$1s^2 2s\ ^2S_{1/2} \rightarrow 1s(2s2p\ ^1P)\ ^2P_{3/2}$ and $1s^2 2s\ ^2S_{1/2} \rightarrow 1s(2s2p\ ^1P)\ ^2P_{1/2}$] are seen in the CRE calculations to increase in intensity relative to the intercombination line as the density increases. When the sum of the calculated intercombination and satellite intensities is compared with the data, measured densities continue to increase for $z < 200$ μm, as shown in Fig. 9.[23] The densities measured in this way are then in reasonable agreement with those measured for $z \leq 100$ μm using technique (2) of the previous paragraph; for $z > 100$ μm, no such comparison is possible, because of insufficient intensity in the helium-like satellite lines.

The density and temperature profiles measured in this way are in fair agreement with those calculated using the two-dimensional hydrodynamics code. Error bars on measured densities are shown only for $z \leq 100$ μm, where they reflect the range of values from the two methods available in that region; error bars for $z > 100$ μm are not necessarily any smaller, but are more difficult to estimate. Even without these experimental uncertainties at the lower densities, agreement in Fig. 9 is seen to be good. Agreement is not quite as good between the calculated and measured temperature profiles in Fig. 9. Temperatures near the target ($z \leq 100$ μm) and beyond the point of peak temperature ($z \geq 400$ μm) are in good agreement, but the details of the intermediate region reveal discrepancies as large as 35%; further comparisons between experiments and calculations will be required to resolve these differences.

To demonstrate that this agreement is sensitive to details of the physics contained in the code, we also show profiles in Fig. 9 from calculations without inverse bremsstrahlung absorption included. Using a simple dump of laser energy at the critical surface, the underdense density and temperature profiles are greatly changed and they no longer agree with the measured profiles. It is interesting to note that the overdense profiles obtained with inverse bremsstrahlung are very similar to those obtained with the critical dump, indicating that overdense profiles are not sensitive to details of the underdense absorption physics.

Comparisons such as these provide the most direct calibration of hydrodynamics codes. Density, temperature, and velocity profiles are the experimental observables most closely coupled to mechanisms of energy absorption and transport in laser-produced plasmas. The ability to reproduce measured profiles is, therefore, a severe test of the ability of the code to treat these physical processes.

DETAILS OF ABSORPTION PHYSICS GREATLY AFFECT DENSITY AND TEMPERATURE PROFILES

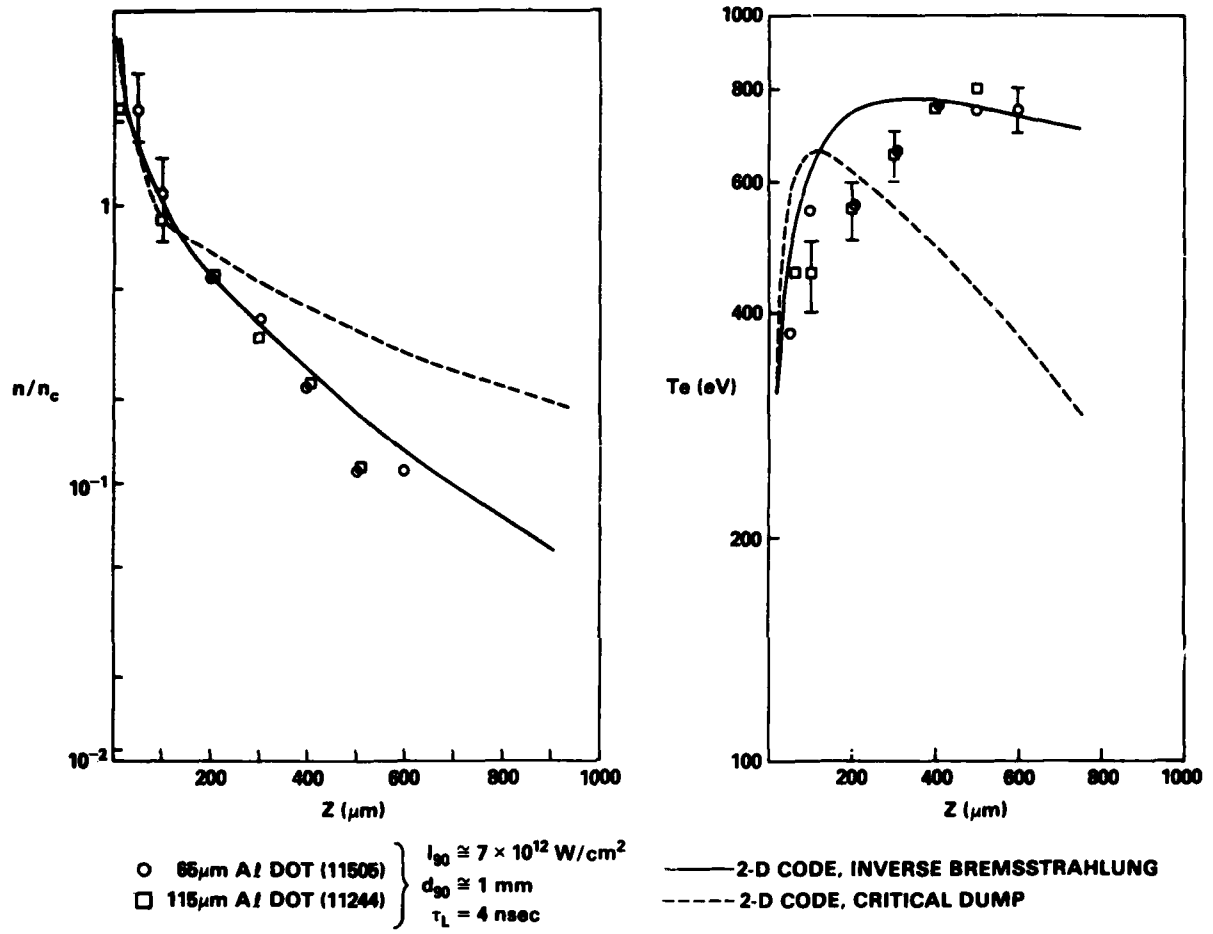

Fig. 9 Data points show density and temperature profiles from spot spectroscopy with 65 μm (o) and 115 μm (□) diameter Al dots. Experimental conditions are $I_{90} \simeq 7 \times 10^{12}$ W/cm^2 within $d_{90} \simeq 1$ mm. 2-D code calculations for the same conditions are shown by the solid curve. The sensitivity of the agreement between code and experiment to details of the code physics is shown by the dotted curve, generated with the 2-D code altered to neglect inverse bremsstrahlung and to dump all energy at critical density.

C. Caveats and Future Work

At least two sets of caveats regarding this work should be pointed out. First, there are three assumptions which we make when reducing the data regarding the spatial qualities of the spectroscopic information. As pointed out in Sec. II.B, the plasma/atomic physics model with which the data are compared simulates a homogeneous cylinder of plasma; the implicit assumption here is that the Al tracer plasma is nearly homogeneous in the radial direction. We also assume that the Al tracer plasma equilibrates with the surrounding CH plasma if tracer spot diameters are kept sufficiently small. This allows us to compare the spectroscopic measurements of density and temperature (which reflect conditions within the Al tracer plasma) with the results of the hydro-code (which simulates a CH target with no Al tracer) in Fig. 9. These first two assumptions seem to be supported by the measured profiles in Fig. 9, where reduced data from two shots with different tracer diameters are shown to agree. A third assumption is that the spectrum emitted at a given distance z from the target is determined by the density and temperature at that position, with negligible effects due to photon pumping from higher density tracer plasma closer to the target. This assumption will be tested using the above-mentioned plasma/atomic physics model.

A second set of caveats concerns the temporal qualities of the spectroscopic information. The present data is time-integrated; in making the comparison in Fig. 9 with an instantaneous profile from the hydro-code (at a time near the peak of the laser pulse), we are implicitly assuming that the hydrodynamics is nearly in steady state. It is appropriate to recall the experimental inferences discussed in Sec. II.A, which support this assumption. By comparing the measurements with a CRE model, we are also making assumptions regarding the steadiness of the atomic physics. As the plasma flows through a given volume at a distance z from the target, we assume that its residence time in that volume is sufficiently long that states of ionization and excitation approach the equilibrium conditions appropriate for $n(z)$ and $T(z)$. This assumption is weakest far from the target surface, where relaxation times increase with decreasing plasma density. In this case, the state of plasma ionization and excitation becomes dependent upon conditions that exist upstream in the hydrodynamic flow, and the temperature determined by spot spectroscopy may reflect an ionization temperature rather than the local electron temperature.

In future work, time-resolved measurements of the profiles should provide a more direct answer to this second set of questions. These measurements, as pointed out in Ref. 2, might be obtained by replacing the film with an x-ray streak camera. An alternative approach is to bury a tracer spot of thickness t at a depth d within the target. By varying the depth d and thickness t of the tracer on a shot-by-shot basis, one may vary the time interval during which the tracer emission occurs.

Future work may also allow us to satisfy the need for measurements of lateral profiles. As mentioned in the introduction, the use of finite focal spots on planar targets causes the problem to become two-dimensional, and simultaneous measurement of axial and lateral profiles is desirable.

By changing the orientation of the spectrograph, one can take full advantage of its two-dimensional imaging capability. Then, using a target identical to those used in flow visualizations (Fig. 1), one obtains an image of the visualized flow in each spectral line detected by the spectrograph. In principle, this technique should allow determination of the desired profiles. Quantitative studies of lateral variations in plasma pressure, as discussed in Sec. II.C, may then be feasible.

IV. LAYERED TRACERS: VELOCITY PROFILE AND ABLATION RATE MEASUREMENTS

Further applications of tracers become available with the use of layered tracer spots. Layered-target methods, suggested originally by G. Dahlbacka and developed by NRL,[24] facilitated studies of axial transport through measurements of mass ablation.[25] Here, we propose the marriage of layered-target techniques with our new tracer methods for measurements of fluid velocity profiles and improved measurements of mass ablation rates.

Use of a layered tracer spot should allow direct and time-resolved measurement of fluid velocity profiles. Before tracers, velocity profiles of the fluid were not measured, despite their importance for interpreting stimulated Brillouin scattering observations. In Ref. 3, we demonstrated an indirect method for inferring time-averaged profiles, but tracers also allow a direct and time-resolved measurement. As shown in Fig. 10, one can fabricate a tracer spot from alternating layers of two materials with distinguishable x-ray emissivities. As each successive layer ablates from the target, the progress through the blowoff plasma of the interface between layers may be observed with an x-ray streak camera; the camera slit is oriented to give spatial resolution along the laser axis. The $z(t)$ curves generated by the multiple interfaces may be inverted to give the velocity profiles $u(z)$ with time resolution.

The above data also yields the ablation rate through each layer of the tracer spot. This is an improvement over the original layered-target measurement of ablation rate,[25] because localization of the layers within the tracer spot alleviates complications due to variations in laser intensity across the irradiated region.

V. SUMMARY

With tracer methods still in their infancy, we see several new techniques which are capable of addressing a variety of interesting and important physics issues. The measurements of density and temperature profiles shown in Sec. II and the proposed measurement of velocity profile discussed in Sec. IV are an important adjunct to experiments related to laser absorption in the underdense plasma. If overdense profiles can be measured with sufficient precision, issues of axial transport of energy inward from the absorption region may be treated; the applicability of the time-resolved ablation rate measurement to this problem is also clear. We have already begun to apply the flow visualization technique to questions of lateral energy spread due to finite focal spot size or due to laser

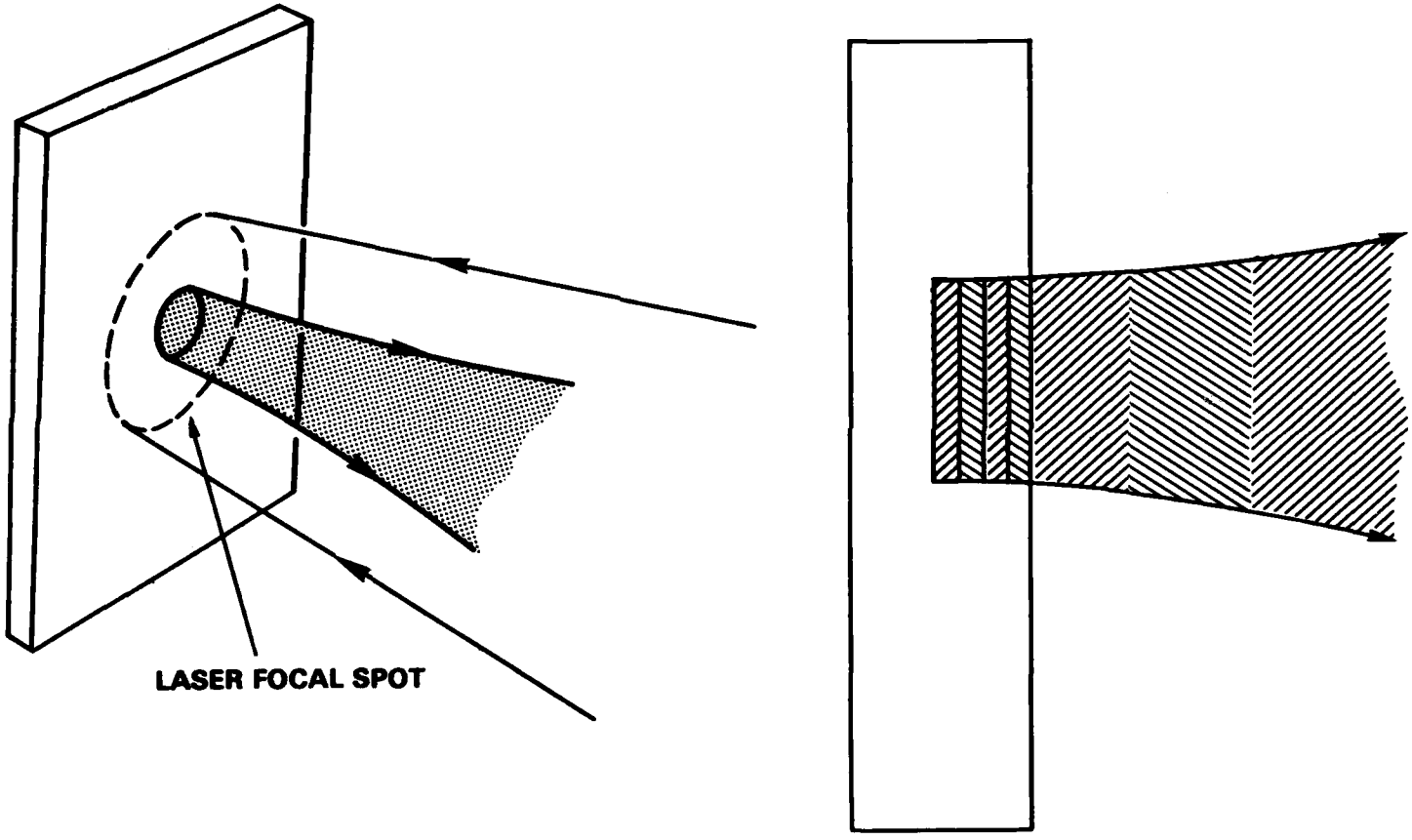

Fig. 10 Illustration of proposed method for time-resolved measurement of velocity profile and for improved ablation rate measurement. At left, the target has a single tracer spot as for spot spectroscopy. The cross-section of the target, at right, shows that the embedded spot is now made of alternating layers of two materials, which ablate sequentially in time during laser irradiation.

nonuniformities, and proposed spectroscopic methods can make this more quantitative. Experiments are also underway to test the use of tracers for detection of Rayleigh-Taylor instability. Many of these measurements provide valuable data for calibration of the hydrodynamics codes upon which we rely for predictions of high-gain target performance. As many of the current ideas for use of tracers are proven and as new ideas continue to surface, we anticipate an expanding role for these methods in experiments related to the physics of laser-matter interaction and to inertial confinement fusion.

VI. ACKNOWLEDGEMENTS

The authors wish to acknowledge useful discussions with Dr. S.E. Bodner, Dr. C.K. Manka, Dr. R.H. Lehmberg, and Dr. H.R. Griem. Invaluable technical support has also been received from M. Fink, E. Turbyfill, N. Nocerino, and J. Kosakowski. This work is supported by the U.S. Department of Energy, Office of Naval Research, and Defense Nuclear Agency.

References

1. M.J. Herbst and J. Grun, Phys. Fluids 24, 1917 (1981).

2. M.J. Herbst, P.G. Burkhalter, J. Grun, R.R. Whitlock, and M. Fink, Rev. Sci. Instr. 53, 1418 (1982).

3. M.J. Herbst, P.G. Burkhalter, J. Grun, S.P. Obenschain, J.A. Stamper, F.C. Young, E.A. McLean, B.H. Ripin, and R.R. Whitlock, NRL Memorandum Report 4893 (1982, unpublished).

4. B.H. Ripin, NRL Memorandum Report 3684 (1977, unpublished).

5. S.P. Obenschain, J. Grun, B.H. Ripin, and E.A. McLean, Phys. Rev. Lett. 46, 1402 (1981).

6. J. Grun, S.P. Obenschain, B.H. Ripin, R.R. Whitlock, E.A. McLean, J. Gardner, M.J. Herbst, and J.A. Stamper, NRL Memorandum Report 4747 (1982, to be published).

7. J. Grun, S.P. Obenschain, R.R. Whitlock, M.J. Herbst, B.H. Ripin, E.A. McLean, M. Emery, and J. Gardner, Bull. Am. Phys. Soc. 26, 1023 (1981); J. Grun, M.J. Herbst, E.A. McLean, S.P. Obenschain, B.H. Ripin, J.A. Stamper, R.R. Whitlock, and F.C. Young, Proc. 12th Anomalous Absorption Conference (1982, to be published).

8. J.H. Gardner, S.E. Bodner, J.P. Boris, M.H. Emery, M. Fritts, and M.J. Herbst, to appear in Laser Interaction and Related Plasma Phenomena, V. 6, ed. H. Hora.

9. M.J. Herbst, J.A. Stamper, R.H. Lehmberg, R.R. Whitlock, F.C. Young, J. Grun, and B.H. Ripin, to appear in Proceedings of the 1981 Topical Conference on Symmetry Aspects of Inertial Fusion Implosions, ed. by S. Bodner, NRL, and NRL Memorandum Report No. 4983.

10. J. Grun, R. Decoste, B.H. Ripin, and J. Gardner, Appl. Phys. Lett. 39, 545 (1981).

11. R.R. Whitlock, S.P. Obenschain, and J. Grun, Appl. Phys. Lett. 41, 429 (1982).

12. M.H. Emery, J.H. Gardner, and J.P. Boris, Phys. Rev. Lett. 48, 677 (1982).

13. B.H. Ripin, S.P. Obenschain, J. Grun, M.J. Herbst, E.A. McLean, J.A. Stamper, R.R. Whitlock, J.M. McMahon, and S.E. Bodner, Bull. Am. Phys. Soc. 25, 946 (1980).

14. H.R. Griem, Plasma Spectroscopy (McGraw-Hill, New York, 1964).

15. D. Duston and J. Davis, Phys. Rev. 21 A, 932 (1980).

16. J.P. Apruzese, P.C. Kepple, K.G. Whitney, J. Davis, and D. Duston, Phys. Rev. 24 A, 1001 (1981).

17. D. Duston, J. Davis, and P.C. Kepple, Phys. Rev. 24 A, 1505 (1981).

18. K.G. Whitney and P.C. Kepple, J. Quant. Spectrosc. Radiat. Transfer 27, 281 (1982).

19. D.B. Brown, J.W. Criss, and L.S. Birks, J. Appl. Phys. 47, 3722 (1976).

20. C.M. Dozier, D.B. Brown, L.S. Birks, P.B. Lyons, and R.F. Benjamin, J. Appl. Phys. 47, 3732 (1976).

21. D. Duston and J. Davis, Phys. Rev. 21 A, 1664 (1980).

22. V.A. Boiko, S.A. Pikuz and A.Ya. Faenov, J. Phys. 12 B, 1889 (1979).

23. P.G. Burkhalter, M.J. Herbst, R.R. Whitlock, and J. Grun, Proceedings 1982 IEEE International Conference on Plasma Science.

24. F.C. Young, R.R. Whitlock, R. Decoste, B.H. Ripin, D.J. Nagel, J.A. Stamper, J.M. McMahon, and S.E. Bodner, Appl. Phys. Lett. 30, 45 (1977).

25. B.H. Ripin, R. Decoste, S.P. Obenschain, S.E. Bodner, E.A. McLean, F.C. Young, R.R. Whitlock, C.M. Armstrong, J. Grun, J.A. Stamper, S.H. Gold, D.J. Nagel, R.H. Lehmberg, and J.M. McMahon, Phys. Fluids 23, 1012 (1980) and 24, 990 (1981).

DISTRIBUTION LIST

University of California
Lawrence Livermore National Lab
Post Office Box 808
Livermore, CA 94550
H.G. Ahlstrom, L-481
J.L Emmett, L-448
J.F. Holzrichter, L-481
M.J. Monsler, L-479
J.H. Nuckolls, L-477
L.W. Coleman, L-473
J.T. Hunt, L-481
A.B. Langdon, L-477

U.S. Department of Energy
Office of Inertial Fusion
Washington, DC 20545
L.E. Killian
G. Gibbs
T.F. Godlove
S.L. Kahalas
J.E. Lewis
R.L. Schriever
T.H. Walsh
S.J. Barish

U.S. Dept. of Energy (194 cys)
Technical Information Center
P.O. Box 62
Oak Ridge, TN 37830

Defense Tech. Information Ctr. (2 cys)
Cameron Station
5010 Duke Street
Alexandria, VA 22314

R. McCrory
University of Rochester
250 East River Road
Rochester, NY 14623

Robert T. Duff
U.S. Department of Energy
Office of Classification
Washington, DC 20545

Rex B. Purcell (2 cys)
U.S. Department of Energy
Nevada Operations Office
Post Office Box 14100
Las Vegas, NV 89114

Z.N. Zafiris/R. Bredderman
U.S. Department of Energy
San Francsico Operations Office
1333 Broadway
Oakland, CA 94512

Los Alamos National Laboratory
Post Office Box 1663
Los Alamos, NM 87545
S.D. Rockwood, ICF Prog. Mgr.
DAD/IF, M/S527 (6 cys)

G. Yonas (4 cys)
Sandia National Laboratories
Post Office Box 5880
Albuquerque, NM 87185

S. Bodner
Naval Research Laboratory
Code 4730
Washington, DC 20375

T. Coffey
Naval Research Laboratory
Code 1001
Washington, DC 20375

Alexander Glass
KMS Fusion, Inc.
3941 Research Park Drive
P.O. Box 1567
Ann Arbor, MI 48106

NRL Code 4700 (26 cys)

NRL Code 4730 (100 cys)

NRL Code 2628 (20 cys)

DEPARTMENT OF DEFENSE

ASSISTANT SECRETARY OF DEFENSE
COMM, CMD, CONT 7 INTELL
WASHINGTON, D.C. 20301

DIRECTOR
COMMAND CONTROL TECHNICAL CENTER
PENTAGON RM BE 685
WASHINGTON, D.C. 20301
01CY ATTN C-650
01CY ATTN C-312 R. MASON

DIRECTOR
DEFENSE ADVANCED RSCH PROJ AGENCY
ARCHITECT BUILDING
1400 WILSON BLVD.
ARLINGTON, VA. 22209
01CY ATTN NUCLEAR MONITORING RESEARCH
01CY ATTN STRATEGIC TECH OFFICE

DEFENSE COMMUNICATION ENGINEER CENTER
1860 WIEHLE AVENUE
RESTON, VA. 22090
01CY ATTN CODE R410
01CY ATTN CODE R812

DEFENSE TECHNICAL INFORMATION CENTER
CAMERON STATION
ALEXANDRIA, VA. 22314
02CY

DIRECTOR
DEFENSE NUCLEAR AGENCY
WASHINGTON, D.C. 20305
01CY ATTN STVL
04CY ATTN TITL
01CY ATTN DDST
03CY ATTN RAAE

COMMANDER
FIELD COMMAND
DEFENSE NUCLEAR AGENCY
KIRTLAND, AFB, NM 87115
01CY ATTN FCPR

DIRECTOR
INTERSERVICE NUCLEAR WEAPONS SCHOOL
KIRTLAND AFB, NM 87115
01CY ATTN DOCUMENT CONTROL

JOINT CHIEFS OF STAFF
WASHINGTON, D.C. 20301
01CY ATTN J-3 WWMCCS EVALUATION OFFICE

DIRECTOR
JOINT STRAT TGT PLANNING STAFF
OFFUTT AFB
OMAHA, NB 68113
01CY ATTN JLTW-2
01CY ATTN JPST G. GOETZ

CHIEF
LIVERMORE DIVISION FLD COMMAND DNA
DEPARTMENT OF DEFENSE
LAWRENCE LIVERMORE LABORATORY
P.O. BOX 808
LIVERMORE, CA 94550
01CY ATTN FCPRL

COMMANDANT
NATO SCHOOL (SHAPE)
APO NEW YORK 09172
01CY ATTN U.S. DOCUMENTS OFFICER

UNDER SECY OF DEF FOR RSCH & ENGRG
DEPARTMENT OF DEFENSE
WASHINGTON, D.C. 20301
01CY ATTN STRATEGIC & SPACE SYSTEMS (OS)

WWMCCS SYSTEM ENGINEERING ORG
WASHINGTON, D.C. 20305
01CY ATTN R. CRAWFORD

COMMANDER/DIRECTOR
ATMOSPHERIC SCIENCES LABORATORY
U.S. ARMY ELECTRONICS COMMAND
WHITE SANDS MISSILE RANGE, NM 88002
01CY ATTN DELAS-EO F. NILES

DIRECTOR
BMD ADVANCED TECH CTR
HUNTSVILLE OFFICE
P.O. BOX 1500
HUNTSVILLE, AL 35807
01CY ATTN ATC-T MELVIN T. CAPPS
01CY ATTN ATC-O W. DAVIES
01CY ATTN ATC-R DON RUSS

PROGRAM MANAGER
BMD PROGRAM OFFICE
5001 EISENHOWER AVENUE
ALEXANDRIA, VA 22333
01CY ATTN DACS-BMT J. SHEA

CHIEF C-E- SERVICES DIVISION
U.S. ARMY COMMUNICATIONS CMD
PENTAGON RM 1B269
WASHINGTON, D.C. 20310
01CY ATTN C- E-SERVICES DIVISION

COMMANDER
FRADCOM TECHNICAL SUPPORT ACTIVITY
DEPARTMENT OF THE ARMY
FORT MONMOUTH, N.J. 07703
01CY ATTN DRSEL-NL-RD H. BENNET
01CY ATTN DRSEL-PL-ENV H. BOMKE
01CY ATTN J.E. QUIGLEY

COMMANDER
HARRY DIAMOND LABORATORIES
DEPARTMENT OF THE ARMY
2800 POWDER MILL ROAD
ADELPHI, MD 20783
(CNWDI-INNER ENVELOPE: ATTN: DELHD-RBH)
01CY ATTN DELHD-TI M. WEINER
01CY ATTN DELHD-RB R. WILLIAMS
01CY ATTN DELHD-NP F. WIMENITZ
01CY ATTN DELHD-NP C. MOAZED

COMMANDER
U.S. ARMY COMM-ELEC ENGRG INSTAL AGY
FT. HUACHUCA, AZ 85613
01CY ATTN CCC-EMEO GEORGE LANE

COMMANDER
U.S. ARMY FOREIGN SCIENCE & TECH CTR
220 7TH STREET, NE
CHARLOTTESVILLE, VA 22901
01CY ATTN DRXST-SD
01CY ATTN R. JONES

COMMANDER
U.S. ARMY MATERIAL DEV & READINESS CMD
5001 EISENHOWER AVENUE
ALEXANDRIA, VA 22333
01CY ATTN DRCLDC J.A. BENDER

COMMANDER
U.S. ARMY NUCLEAR AND CHEMICAL AGENCY
7500 BACKLICK ROAD
BLDG 2073
SPRINGFIELD, VA 22150
01CY ATTN LIBRARY

DIRECTOR
U.S. ARMY BALLISTIC RESEARCH LABORATORY
ABERDEEN PROVING GROUND, MD 21005
01CY ATTN TECH LIBRARY EDWARD BAICY

COMMANDER
U.S. ARMY SATCOM AGENCY
FT. MONMOUTH, NJ 07703
01CY ATTN DOCUMENT CONTROL

COMMANDER
U.S. ARMY MISSILE INTELLIGENCE AGENCY
REDSTONE ARSENAL, AL 35809
01CY ATTN JIM GAMBLE

DIRECTOR
U.S. ARMY TRADOC SYSTEMS ANALYSIS ACTIVITY
WHITE SANDS MISSILE RANGE, NM 88002
01CY ATTN ATAA-SA
01CY ATTN TCC/F. PAYAN JR.
01CY ATTN ATTA-TAC LTC J. HESSE

COMMANDER
NAVAL ELECTRONIC SYSTEMS COMMAND
WASHINGTON, D.C. 20360
01CY ATTN NAVALEX 034 T. HUGHES
01CY ATTN PME 117
01CY ATTN PME 117-T
01CY ATTN CODE 5011

COMMANDING OFFICER
NAVAL INTELLIGENCE SUPPORT CTR
4301 SUITLAND ROAD, BLDG. 5
WASHINGTON, D.C. 20390
01CY ATTN MR. DUBBIN STIC 12
01CY ATTN NISC-50
01CY ATTN CODE 5404 J. GALET

COMMANDER
NAVAL OCCEAN SYSTEMS CENTER
SAN DIEGO, CA 92152
03CY ATTN CODE 532 W. MOLER
01CY ATTN CODE 0230 C. BAGGETT
01CY ATTN CODE 81 R. EASTMAN

DIRECTOR
NAVAL RESEARCH LABORATORY
WASHINGTON, D.C. 20375
01CY ATTN CODE 4700 S. L. Ossakow
26 CYS IF UNCLASS. 1 CY IF CLASS)
01CY ATTN CODE 4701 JACK D. BROWN
01CY ATTN CODE 4780 BRANCH HEAD (100
CYS IF UNCLASS, 1 CY IF CLASS)
01CY ATTN CODE 7500
01CY ATTN CODE 7550
01CY ATTN CODE 7580
01CY ATTN CODE 7551
01CY ATTN CODE 7555
01CY ATTN CODE 4730 E. MCLEAN
01CY ATTN CODE 4187

COMMANDER
NAVAL SEA SYSTEMS COMMAND
WASHINGTON, D.C. 20362
01CY ATTN CAPT R. PITKIN

COMMANDER
NAVAL SPACE SURVEILLANCE SYSTEM
DAHLGREN, VA 22448
01CY ATTN CAPT J.H. BURTON

OFFICER-IN-CHARGE
NAVAL SURFACE WEAPONS CENTER
WHITE OAK, SILVER SPRING, MD 20910
01CY ATTN CODE F31

DIRECTOR
STRATEGIC SYSTEMS PROJECT OFFICE
DEPARTMENT OF THE NAVY
WASHINGTON, D.C. 20376
01CY ATTN NSP-2141
01CY ATTN NSSP-2722 FRED WIMBERLY

COMMANDER
NAVAL SURFACE WEAPONS CENTER
DAHLGREN LABORATORY
DAHLGREN, VA 22448
01CY ATTN CODE DF-14 R. BUTLER

OFFICER OF NAVAL RESEARCH
ARLINGTON, VA 22217
01CY ATTN CODE 465
01CY ATTN CODE 461
01CY ATTN CODE 402
01CY ATTN CODE 420
01CY ATTN CODE 421

COMMANDER
AEROSPACE DEFENSE COMMAND/DC
DEPARTMENT OF THE AIR FORCE
ENT AFB, CO 80912
01CY ATTN DC· MR. LONG

COMMANDER
AEROSPACE DEFENSE COMMAND/XPD
DEPARTMENT OF THE AIR FORCE
ENT AFB, CO 80912
01CY ATTN XPDQQ
01CY ATTN XP

AIR FORCE GEOPHYSICS LABORATORY
HANSCOM AFB, MA 01731
01CY ATTN OPR HAROLD GARDNER
01CY ATTN LKB KENNETH S.W. CHAMPION
01CY ATTN OPR ALVA T. STAIR
01CY ATTN PHP JULES AARONS
01CY ATTN PHD JURGEN BUCHAU
01CY ATTN PHD JOHN P. MULLEN

AF WEAPONS LABORATORY
KIRTLAND AFT, NM 87117
01CY ATTN SUL
01CY ATTN CA ARTHUR H. GUENTHER
01CY ATTN NTYCE 1LT. G. KRAJEI

AFTAC
PATRICK AFB, FL 32925
01CY ATTN TF/MAJ WILEY
01CY ATTN TN

AIR FORCE AVIONICS LABORATORY
WRIGHT-PATTERSON AFB, OH 45433
01CY ATTN AAD WADE HUNT
01CY ATTN AAD ALLEN JOHNSON

DEPUTY CHIEF OF STAFF
RESEARCH, DEVELOPMENT, & ACQ
DEPARTMENT OF THE AIR FORCE
WASHINGTON, D.C. 20330
01CY ATTN AFRDQ

HEADQUATERS
ELECTRONIC SYSTEMS DIVISION/XR
DEPARTMENT OF THE AIR FORCE
HANSCOM AFB, MA 01731
01CY ATTN XR J. DEAS

HEADQUATERS
ELECTRONIC SYSTEMS DIVISION/YSEA
DEPARTMENT OF THE AIR FORCE
HANSCOM AFB, MA 01732
01CY ATTN YSEA

HEADQUATERS
ELECTRONIC SYSTEMS DIVISION/DC
DEPARTMENT OF THE AIR FORCE
HANSCOM AFB, MA 01731
01CY ATTN DCKC MAJ J.C. CLARK

COMMANDER
FOREIGN TECHNOLOGY DIVISION, AFSC
WRIGHT-PATTERSON AFB, OH 45433
01CY ATTN NICD LIBRARY
01CY ATTN ETDP B. BALLARD

COMMANDER
ROME AIR DEVELOPMENT CENTER, AFSC
GRIFFISS AFB, NY 13441
01CY ATTN DOC LIBRARY/TSLD
01CY ATTN OCSE V. COYNE

SAMSO/SZ
POST OFFICE BOX 92960
WORLDWAY POSTAL CENTER
LOS ANGELES, CA 90009
(SPACE DEFENSE SYSTEMS)
01CY ATTN SZJ

STRATEGIC AIR COMMAND/XPFS
OFFUTT AFB, NB 68113
01CY ATTN XPFS MAJ B. STEPHAN
01CY ATTN ADWATE MAJ BRUCE BAUER
01CY ATTN NRT
01CY ATTN DOK CHIEF SCIENTIST

SAMSO/SK
P.O. BOX 92960
WORLDWAY POSTAL CENTER
LOS ANGELES, CA 90009
01CY ATTN SKA (SPACE COMM SYSTEMS)
M. CLAVIN

SAMSO/MN
NORTON AFB, CA 92409
(MINUTEMAN)
01CY ATTN MNNL LTC KENNEDY

COMMANDER
ROME AIR DEVELOPMENT CENTER, AFSC
HANSCOM AFB, MA 01731
01CY ATTN EEP A. LORENTZEN

DEPARTMENT OF ENERGY
LIBRARY ROOM G-042
WASHINGTON, D.C. 20545
01CY ATTN DOC CON FOR A. LABOWITZ

DEPARTMENT OF ENERGY
ALBUQUERQUE OPERATIONS OFFICE
P.O. BOX 5400
ALBUQUERQUE, NM 87115
01CY ATTN DOC CON FOR D. SHERWOOD

EG&G, INC.
LOS ALAMOS DIVISION
P.O. BOX 809
LOS ALAMOS, NM 85544
01CY ATTN DOC CON FOR J. BREEDLOVE

UNIVERSITY OF CALIFORNIA
LAWRENCE LIVERMORE LABORATORY
P.O. BOX 808
LIVERMORE, CA 94550
01CY ATTN DOC CON FOR TECH INFO DEPT
01CY ATTN DOC CON FOR L-389 R. OTT
01CY ATTN DOC CON FOR L-31 R. HAGER
01CY ATTN DOC CON FOR L-46 F. SEWARD

LOS ALAMOS NATIONAL LABORATORY
P.O. BOX 1663
LOS ALAMOS, NM 87545
01CY ATTN DOC CON FOR J. WOLCOTT
01CY ATTN DOC CON FOR R.F. TASCHEK
01CY ATTN DOC CON FOR E. JONES
01CY ATTN DOC CON FOR J. MALIK
01CY ATTN DOC CON FOR R. JEFFRIES
01CY ATTN DOC CON FOR J. ZINN
01CY ATTN DOC CON FOR P. KEATON
01CY ATTN DOC CON FOR D. WESTERVELT

SANDIA LABORATORIES
P.O. BOX 5800
ALBUQUERQUE, NM 87115
01CY ATTN DOC CON FOR W. BROWN
01CY ATTN DOC CON FOR A. THORNBROUGH
01CY ATTN DOC CON FOR T. WRIGHT
01CY ATTN DOC CON FOR D. DAHLGREN
01CY ATTN DOC CON FOR 3141
01CY ATTN DOC CON FOR SPACE PROJECT DIV

SANDIA LABORATORIES
LIVERMORE LABORATORY
P.O. BOX 969
LIVERMORE, CA 94550
01CY ATTN DOC CON FOR B. MURPHEY
01CY ATTN DOC CON FOR T. COOK

OFFICE OF MILITARY APPLICATION
DEPARTMENT OF ENERGY
WASHINGTON, D.C. 20545
01CY ATTN DOC CON DR. YO SONG

OTHER GOVERNMENT

DEPARTMENT OF COMMERCE
NATIONAL BUREAU OF STANDARDS
WASHINGTON, D.C. 20234
(ALL CORRES: ATTN SEC OFFICER FOR)
01CY ATTN R. MOORE

INSTITUTE FOR TELECOM SCIENCES
NATIONAL TELECOMMUNICATIONS & INFO ADMIN
BOULDER, CO 80303
01CY ATTN A. JEAN (UNCLASS ONLY)
01CY ATTN W. UTLAUT
01CY ATTN D. CROMBIE
01CY ATTN L. BERRY

NATIONAL OCEANIC & ATMOSPHERIC ADMIN
ENVIRONMENTAL RESEARCH LABORATORIES
DEPARTMENT OF COMMERCE
BOULDER, CO 80302
01CY ATTN R. GRUBB
01CY ATTN AERONOMY LAB G. REID

DEPARTMENT OF DEFENSE CONTRACTORS

AEROSPACE CORPORATION
P.O. BOX 92957
LOS ANGELES, CA 90009
01CY ATTN I. GARFUNKEL
01CY ATTN T. SALMI
01CY ATTN V. JOSEPHSON
01CY ATTN S. BOWER
01CY ATTN D. OLSEN

ANALYTICAL SYSTEMS ENGINEERING CORP
5 OLD CONCORD ROAD
BURLINGTON, MA 01803
01CY ATTN RADIO SCIENCES

BERKELEY RESEARCH ASSOCIATES, INC.
P.O. BOX 983
BERKELEY, CA 94701
01CY ATTN J. WORKMAN
01CY ATTN C. PRETTIE
01CY ATTN S. BRECHT

BOEING COMPANY, THE
P.O. BOX 3707
SEATTLE, WA 98124
01CY ATTN G. KEISTER
01CY ATTN D. MURRAY
01CY ATTN G. HALL
01CY ATTN J. KENNEY

CALIFORNIA AT SAN DIEGO, UNIV OF
P.O. BOX 6049
SAN DIEGO, CA 92106

CHARLES STARK DRAPER LABORATORY, INC.
555 TECHNOLOGY SQUARE
CAMBRIDGE, MA 02139
01CY ATTN D.B. COX
01CY ATTN J.P. GILMORE

COMSAT LABORATORIES
LINTHICUM ROAD
CLARKSBURG, MD 20734
01CY ATTN G. HYDE

CORNELL UNIVERSITY
DEPARTMENT OF ELECTRICAL ENGINEERING
ITHACA, NY 14850
01CY ATTN D.T. FARLEY, JR.

ELECTROSPACE SYSTEMS, INC.
BOX 1359
RICHARDSON, TX 75080
01CY ATTN H. LOGSTON
01CY ATTN SECURITY (PAUL PHILLIPS)

ESL, INC.
495 JAVA DRIVE
SUNNYVALE, CA 94086
01CY ATTN J. ROBERTS
01CY ATTN JAMES MARSHALL

GENERAL ELECTRIC COMPANY
SPACE DIVISION
VALLEY FORGE SPACE CENTER
GODDARD BLVD KING OF PRUSSIA
P.O. BOX 8555
PHILADELPHIA, PA 19101
01CY ATTN M.H. BORTNER SPACE SCI LAB

GENERAL ELECTRIC COMPANY
P.O. BOX 1122
SYRACUSE, NY 13201
01CY ATTN F. REIBERT

GENERAL ELECTRIC TECH SERVICES CO., INC.
HMES
COURT STREET
SYRACUSE, NY 13201
01CY ATTN G. MILLMAN

GENERAL RESEARCH CORPORATION
SANTA BARBARA DIVISION
P.O. BOX 6770
SANTA BARBARA, CA 93111
01CY ATTN JOHN ISE, JR.
01CY ATTN JOEL GARBARINO

GEOPHYSICAL INSTITUTE
UNIVERSITY OF ALASKA
FAIRBANKS, AK 99701
(ALL CLASS ATTN: SECURITY OFFICER)
01CY ATTN T.N. DAVIS (UNCLASS ONLY)
01CY ATTN TECHNICAL LIBRARY
01CY ATTN NEAL BROWN (UNCLASS ONLY)

GTE SYLVANIA, INC.
ELECTRONICS SYSTEMS GRP-EASTERN DIV
77 A STREET
NEEDHAM, MA 02194
01CY ATTN MARSHALL CROSS

HSS, INC.
2 ALFRED CIRCLE
BEDFORD, MA 01730
01CY ATTN DONALD HANSEN

ILLINOIS, UNIVERSITY OF
107 COBLE HALL
150 DAVENPORT HOUSE
CHAMPAIGN, IL 61820
(ALL CORRES ATTN DAN MCCLELLAND)
01CY ATTN K. YEH

INSTITUTE FOR DEFENSE ANALYSES
400 ARMY-NAVY DRIVE
ARLINGTON, VA 22202
01CY ATTN J.M. AEIN
01CY ATTN ERNEST BAUER
01CY ATTN HANS WOLFARD
01CY ATTN JOEL BENGSTON

INTL TEL & TELEGRAPH CORPORATION
500 WASHINGTON AVENUE
NUTLEY, NJ 07110
01CY ATTN TECHNICAL LIBRARY

JAYCOR
11011 TORREYANA ROAD
P.O. BOX 85154
SAN DIEGO, CA 92138
01CY ATTN J.L. SPERLING

JOHNS HOPKINS UNIVERSITY
APPLIED PHYSICS LABORATORY
JOHNS HOPKINS ROAD
LAURAL, MD 20810
01CY ATTN DOCUMENT LIBRARIAN
01CY ATTN THOMAS POTEMRA
01CY ATTN JOHN DASSOULAS

KAMAN SCIENCES CORP
P.O. BOX 7463
COLORADO SPRINGS, CO 80933
01CY ATTN T. MEAGHER
KAMAN TEMPO-CENTER FOR ADVANCED STUDIES
816 STATE STREET (P.O DRAWER QQ)
SANTA BARBARA, CA 93102
01CY ATTN DASIAC
01CY ATTN TIM STEPHANS
01CY ATTN WARREN S. KNAPP
01CY ATTN WILLIAM MCNAMARA
01CY ATTN B. GAMBILL

LINKABIT CORP
10453 ROSELLE
SAN DIEGO, CA 92121
01CY ATTN IRWIN JACOBS

LOCKHEED MISSILES & SPACE CO., INC
P.O. BOX 504
SUNNYVALE, CA 94088
01CY ATTN DEPT 60-12
01CY ATTN D.R. CHURCHILL

LOCKHEED MISSILES & SPACE CO., INC.
3251 HANOVER STREET
PALO ALTO, CA 94304
01CY ATTN MARTIN WALT DEPT 52-12
01CY ATTN W.L. IMHOF DEPT 52-12
01CY ATTN RICHARD G. JOHNSON DEPT 52-1
01CY ATTN J.B. CLADIS DEPT 52-12

LOCKHEED MISSILE & SPACE CO., INC.
HUNTSVILLE RESEARCH & ENGR. CTR.
4800 BRADFORD DRIVE
HUNTSVILLE, AL 35807
ATTN DALE H. DIVIS

MARTIN MARIETTA CORP
ORLANDO DIVISION
P.O. BOX 5837
ORLANDO, FL 32805
01CY ATTN R. HEFFNER

M.I.T. LINCOLN LABORATORY
P.O. BOX 73
LEXINGTON, MA 02173
01CY ATTN DAVID M. TOWLE
01CY ATTN P. WALDRON
01CY ATTN L. LOUGHLIN
01CY ATTN D. CLARK

MCDONNEL DOUGLAS CORPORATION
5301 BOLSA AVENUE
HUNTINGTON BEACH, CA 92647
01CY ATTN N. HARRIS
01CY ATTN J. MOULE
01CY ATTN GEORGE MROZ
01CY ATTN W. OLSON
01CY ATTN R.W. HALPRIN
01CY ATTN TECHNICAL LIBRARY SERVICES

MISSION RESEARCH CORPORATION
735 STATE STREET
SANTA BARBARA, CA 93101
01CY ATTN P. FISCHER
01CY ATTN W.F. CREVIER
01CY ATTN STEVEN L. GUTSCHE
01CY ATTN D. SAPPENFIELD
01CY ATTN R. BOGUSCH
01CY ATTN R. HENDRICK
01CY ATTN RALPH KILB
01CY ATTN DAVE SOWLE
01CY ATTN F. FAJEN
01CY ATTN M. SCHEIBE
01CY ATTN CONRAD L. LONGMIRE
01CY ATTN WARREN A. SCHLUETER

MITRE CORPORATION, THE
P.O. BOX 208
BEDFORD, MA 01730
01CY ATTN JOHN MORGANSTERN
01CY ATTN G. HARDING
01CY ATTN C.E. CALLAHAN

MITRE CORP
WESTGATE RESEARCH PARK
1820 DOLLY MADISON BLVD
MCLEAN, VA 22101
01CY ATTN W. HALL
01CY ATTN W. FOSTER

PACIFIC-SIERRA RESEARCH CORP
12340 SANTA MONICA BLVD.
LOS ANGELES, CA 90025
01CY ATTN E.C. FIELD, JR.

PENNSYLVANIA STATE UNIVERSITY
IONOSPHERE RESEARCH LAB
318 ELECTRICAL ENGINEERING EAST
UNIVERSITY PARK, PA 16802
(NO CLASS TO THIS ADDRESS)
01CY ATTN IONOSPHERIC RESEARCH LAB

PHOTOMETRICS, INC.
442 MARRETT ROAD
LEXINGTON, MA 02173
01CY ATTN IRVING L. KOFSKY

PHYSICAL DYNAMICS, INC.
P.O. BOX 3027
BELLEVUE, WA 98009
01CY ATTN E.J. FREMOUW

PHYSICAL DYNAMICS, INC.
P.O. BOX 10367
OAKLAND, CA 94610
ATTN A. THOMSON

R & D ASSOCIATES
P.O. BOX 9695
MARINA DEL REY, CA 90291
01CY ATTN FORREST GILMORE
01CY ATTN WILLIAM B. WRIGHT, JR.
01CY ATTN ROBERT F. LELEVIER
01CY ATTN WILLIAM J. KARZAS
01CY ATTN H. ORY
01CY ATTN C. MACDONALD
01CY ATTN R. TURCO

RAND CORPORATION, THE
1700 MAIN STREET
SANTA MONICA, CA 90406
01CY ATTN CULLEN CRAIN
01CY ATTN ED BEDROZIAN

RAYTHEON CO.
528 BOSTON POST ROAD
SUDBURY, MA 01776
01CY ATTN BARBARA ADAMS

RIVERSIDE RESEARCH INSTITUTE
80 WEST END AVENUE
NEW YORK, NY 10023
01CY ATTN VINCE TRAPANI

SCIENCE APPLICATIONS, INC.
P.O. BOX 2351
LA JOLLA, CA 92038
01CY ATTN LEWIS M. LINSON
01CY ATTN DANIEL A. HAMLIN
01CY ATTN E. FRIEMAN
01CY ATTN E.A. STRAKER
01CY ATTN CURTIS A. SMITH
01CY ATTN JACK MCDOUGALL

SCIENCE APPLICATIONS, INC
1710 GOODRIDGE DR.
MCLEAN, VA 22102
ATTN: J. COCKAYNE

SRI INTERNATIONAL
333 RAVENSWOOD AVENUE
MENLO PARK, CA 94025
01CY ATTN DONALD NEILSON
01CY ATTN ALAN BURNS
01CY ATTN G. SMITH
01CY ATTN L.L. COBB
01CY ATTN DAVID A. JOHNSON
01CY ATTN WALTER G. CHESNUT
01CY ATTN CHARLES L. RINO
01CY ATTN WALTER JAYE
01CY ATTN M. BARON
01CY ATTN RAY L. LEADABRAND
01CY ATTN G. CARPENTER
01CY ATTN G. PRICE
01CY ATTN J. PETERSON
01CY ATTN R. HAKE, JR.
01CY ATTN V. GONZALES
01CY ATTN D. MCDANIEL

STEWART RADIANCE LABORATORY
UTAH STATE UNIVERSITY
1 DE ANGELO DRIVE
BEDFORD, MA 01730
01CY ATTN J. ULWICK

TECHNOLOGY INTERNATIONAL CORP
75 WIGGINS AVENUE
BEDFORD, MA 01730
01CY ATTN W.P. BOQUIST

TRW DEFENSE & SPACE SYS GROUP
ONE SPACE PARK
REDONDO BEACH, CA 90278
01CY ATTN R. K. PLEBUCH
01CY ATTN S. ALTSCHULER
01CY ATTN D. DEE
01CY ATTN D/STOCKWELL
SNTF/1575

VISIDYNE
SOUTH BEDFORD STREET
BURLINGTON, MASS 01803
01CY ATTN W. REIDY
01CY ATTN J. CARPENTER
01CY ATTN C. HUMPHREY

EOS TECHNOLOGIES, INC.
606 Wilshire Blvd.
Santa Monica, Calif 90401
01CY ATTN C.B. GABBARD